NON-ADIABATIC BLOWDOWN MODEL: A COMPLIMENTARY TOOL FOR THE SAFETY DESIGN OF TANK-TPRD SYSTEM

Dadashzadeh, M., Makarov, D. and Molkov, V.
[1] Hydrogen Safety Engineering and Research Centre (HySAFER), Ulster University, Shore Road, Newtownabbey, Co. Antrim, BT37 0QB, UK, s.dadashzadeh@ulster.ac.uk

ABSTRACT

Previous studies have demonstrated that while blowdown pressure is reproduced well by both adiabatic and isothermal analytical models, the dynamics of temperature cannot be predicted well by either model. The reason for the last is heat transfer to cooling during expansion gas from the vessel wall. Moreover, when exposed to an external fire, the temperature inside the vessel increases, i.e. when a thermally activated pressure relief device (TPRD) is still closed, with subsequent pressure increase that may lead to a catastrophic rupture of the vessel. The choice of a TPRD exit orifice size and design strategy are challenges: to provide sufficient internal pressure drop in a fire when the orifice size is too small; to avoid flame blow off expected with the decrease of pressure during the blowdown; to decrease flame length of subsequent jet fire as much as possible by the decrease of the orifice size under condition of sufficient fire resistance provisions, to avoid pressure peaking phenomenon, etc. The adiabatic model of blowdown [1] was developed using the Abel-Nobel equation of state and the original theory of under-expanded jet [2]. According to experimental observations, e.g. [3], heat transfer plays a significant role during the blowdown. Thus, this study aims to modify the adiabatic blowdown model to include the heat transfer to non-ideal gas. The model accounts for a change of gas temperature inside the vessel due to two "competing" processes: the decrease of temperature due to gas expansion and the increase of temperature due to heat transfer from the surroundings, e.g. ambience or fire, through the vessel wall. This is taken into account in the system of equations of adiabatic blowdown model through the change of energy conservation equation that accounts for heat from outside. There is a need to know the convective heat transfer coefficient between the vessel wall and the surroundings and wall size and properties to define heat flux to the gas inside the vessel. The non-adiabatic model is validated against available experimental data. The model can be applied as a new engineering tool for the inherently safer design of hydrogen tank-TPRD system.

Nomenclature

A	Surface of the metal plate on top of thermocouple, m^2
A_{int}	Internal surface of the tank, m^2
b	Co-volume constant of the gas for Abel-Noble equation, $m^3\ kg^{-1}$
C_D	Discharge coefficient
$c_{p,\ air}$	Specific heat capacity of air, $J\ kg^{-1}\ K^{-1}$
$c_{p,\ CFRP}$	Specific heat capacity of CFRP, $J\ kg^{-1}\ K^{-1}$
$c_{p,\ Liner}$	Specific heat capacity of liner, $J\ kg^{-1}\ K^{-1}$
$c_{p,\ plate}$	Specific heat capacity of the metal plate on top of thermocouple, $J\ kg^{-1}\ K^{-1}$
$c_{p,g}$	Specific heat capacity of the inside gas at constant pressure, $J\ kg^{-1}\ K^{-1}$
$c_{v,g}$	Specific heat capacity of the inside gas at constant volume, $J\ kg^{-1}\ K^{-1}$
$c_{w(n)}$	Specific heat capacity of the wall (Liner or CFRP) at grid point n, $J\ kg^{-1}\ K^{-1}$
D_2	Diameter of the orifice, m
D_3	Diameter of the effective nozzle, m
D_{ext}	External diameter of the tank, m
D_{int}	Inside diameter of the tank, m
D_{plate}	Diameter of the metal plate on top of thermocouple, m
g	Acceleration due to gravity, $m\ s^{-2}$
h_{out}	Enthalpy going out, $J\ kg^{-1}$
i	Iteration number, -
k_{ext}	Heat transfer coefficient of the external surface of the wall, $W\ m^{-2}\ K^{-1}$
k_{int}	Heat transfer coefficient of the internal surface of the wall, $W\ m^{-2}\ K^{-1}$
k_{plate}	Heat transfer coefficient of the metal plate on top of thermocouple, $W\ m^{-2}\ K^{-1}$
m_1	Mass in the vessel, kg
n	Grid point number, -
L	Thickness of the metal plate on top of thermocouple, m
M_g	Inside gas molar mas, $g\ mol^{-1}$
Nu_{Dext}	Nusselt number of the air, -
Nu_{Dint}	Nusselt number of the inside gas, -

Nu_{plate}	Nusselt number of the metal plate on top of thermocouple, -
P_1	Pressure of the gas inside the tank, Pa
P_2	Pressure of the gas at the orifice, Pa
P_{amb}	Ambient pressure, Pa
Pr_{air}	Prandtl number of the air
Q	Heat to the system due to surrounding, J
Ra_{Dint}	Rayleigh number of the inside gas, -
Ra_{plate}	Rayleigh number of the metal plate on top of thermocouple, -
Re_{Dext}	Reynolds number of the air, -
R_g	Gas constant, $m^2\ s^2\ K^{-1}$
S	Source term, $W\ m^{-3}\ s^{-1}$
t	Time, s
T_1	Temperature of the gas inside the tank, K
T_2	Temperature of the gas at the orifice, K
T_3	Temperature at the notional nozzle, K
T_{amb}	Ambient temperature, K
T_{plate}	Temperature of the metal plate on top of thermocouple, K
$T_{w(ext)}$	Temperature of the external surface of the tank, K
$T_{w(int)}$	Temperature of the internal surface of the tank, K
$T_{w(int)}$	Temperature of the internal surface of the tank, K
$T_{w(n)}$	Temperature of wall at the grid-point n, K
$T_{w(N)}$	Temperature of the last grid point before the external surface, K
U	Internal energy in the tank, J
u_2	Velocity in orifice, $m\ s^{-1}$
u_3	Velocity at the notional nozzle, $m\ s^{-1}$
V	Volume of the tank, m^3
V_{air}	Velocity of surrounding air, $m\ s^{-1}$
V_{plate}	Volume of the metal plate on top of thermocouple, m^3
$\Delta\bar{x}_{ext}$	Distance from grid point n to the external surface of the control volume, m

Δx_{ext}^{+} Distance from the external surface of the control volume to the grid point n+1, m

Δx_{int}^{-} Distance from the internal surface of the control volume to the grid point n-1, m

Δx_{int}^{+} Distance from grid point n to the internal surface of the control volume, m

λ_{ext}^{-} Thermal conductivity of the wall between grid point n and the external surface of the control volume, W m^{-1} K^{-1}

λ_{ext}^{+} Thermal conductivity of the wall between the external surface of the control volume and grid point n+1, W m^{-1} K^{-1}

λ_{int}^{-} Thermal conductivity of the wall between the internal surface of the control volume and grid point n-1, W m^{-1} K^{-1}

λ_{int}^{+} Thermal conductivity of the wall between grid point n and the internal surface of the control volume, W m^{-1} K^{-1}

$\dot{m}$ Mass flow rate, kg s^{-1}

Δx Length of control volumes, m

β Thermal expansion coefficient of the gas, K^{-1}

γ Ratio of the specific heat capacity, -

λ_{air} Thermal conductivity of ambience, W m^{-1} K^{-1}

λ_{CFRP} Thermal conductivity of CFRP, W m^{-1} K^{-1}

λg Thermal conductivity of the gas, W m^{-1} K^{-1}

λ_{Liner} Thermal conductivity of Liner, W m^{-1} K^{-1}

μ_{air} Viscosity of air, Pa s

μ_g Dynamic viscosity of the gas, Pa s

ρ_1 Density of the gas inside the tank, kg m^{-3}

ρ_2 Density of the gas at the orifice, kg/m^3

ρ_3 Density at the notional nozzle, kg m^{-3}

ρ_{air} Density of air, kg m^{-3}

ρ_{CFRP} Density of CFRP, kg m^{-3}

ρ_{Liner} Density of liner, kg m^{-3}

ρ_{plate} Density of the metal plate on top of thermocouple, kg m^{-3}

$\rho_{w(n)}$ Density of the wall (Liner or CFRP) at grid point n, kg m^{-3}

1.0 INTRODUCTION

Hydrogen is stored onboard in composite vessels at nominal working pressure of 35 MPa (buses) to 70 MPa (cars). Being exposed to an external fire, the inside temperature and pressure of the tank start to grow. Due to the high temperature from the fire, the external side of the wall starts to be degraded and tank loses its load bearing ability over the time. Eventually, when the degradation temperature reaches to a certain thickness of the tank wall, rupture occurs with its subsequent catastrophic consequences, i.e. overpressure due to the blast wave or thermal hazards due to the fireball [4]. The regulations require TPRD to be installed on hydrogen onboard tanks to prevent its catastrophic rupture in a fire. In case of high fire temperatures TPRD must be activated and it is intended to provide a release of hydrogen from the tank before its rupture. When the blowdown starts, the inside temperature of the tank decreases due to the depressurization. Thus, the heat transfer within the tank wall and the wall degradation is now affected by two competing waves: the increase of the wall temperature due to the external high temperature; the decrease of the wall temperature due to the temperature drop of the inside gas. Thus, the wall degradation is now slower if it is not stopped!!!

Safety design of tank-TPRD system is a complicated task with various parameters which are vital to be carefully addressed, i.e. the volume of the pressurised tank and its storage pressure, the diameter of TPRD, the initiating time of TPRD, heat transfer through the wall from the external fire and from the inside gas, wall degradation due to the fire, etc. Investigating above phenomena with experimental tools is an expensive approach. Computational fluid dynamics (CFD) simulation is an alternative method to avoid the expensive and risky experiments. However, it must be recalled that due to the interaction of various phenomena and their complexities, the CFD simulation is not time efficient: days for a 2D simulation to a month for 3D simulation [5].

To predict the pressure and temperature change inside an extremely pressurised tank, a dynamic notional nozzle model was developed by [1]. The model was based on Abel-Nobel equation of state and conservation equations of mass and total energy and it was validated against experiments. The previous version of the model was applicable for two cases of adiabatic discharge (no heat transfer) and discharge under the constant temperature conditions (ideal heat transfer) [1]. The effect of various heat transfer boundary conditions on the blowdown dynamic was comprehensively investigated by [3]. It was concluded that the heat transfer due to ambience/fire plays a significant role during the blowdown.

The present study aims to incorporate the developed and experimentally validated correlations to build an engineering tool for the safety design of pressurised tank-TPRD system. The model considers the heat transfer phenomenon within the tank wall which is due to heating up (ambience/external fire) and cooling down (internal depressurisation). The TPRD optimum orifice size and its activation time are also effective players which are considered in the tool. Predicting the dynamic pressure and temperature of the tank during blowdown are addressed within the development of the tool.

To do so, a novel blowdown model is introduced in which the dynamic pressure and temperature inside the tank is predicted by employing the energy conservation equation and the real gas equation of state. The underexpanded jet theory [1] is used for analysing the gas behaviour within the TPRD orifice and after the exit. Heat transfer through the tank wall is addressed by exploiting one dimensional unsteady heat transfer equation and the system of equations are solved by employing the finite-difference method [6]. For the natural and enforced convection, Nusselt number correlations are used to calculate the heat transfer coefficients [7].

2.0 MODEL EXPLAINATION

To calculate the dynamic temperature and pressure inside the tank, the systems of equations are solved in three steps: inside the tank (1 in Fig. 1a); at the orifice (2 in Fig. 1a) and the notional nozzle (3 in Fig. 1a); within the wall (Fig. 1b).

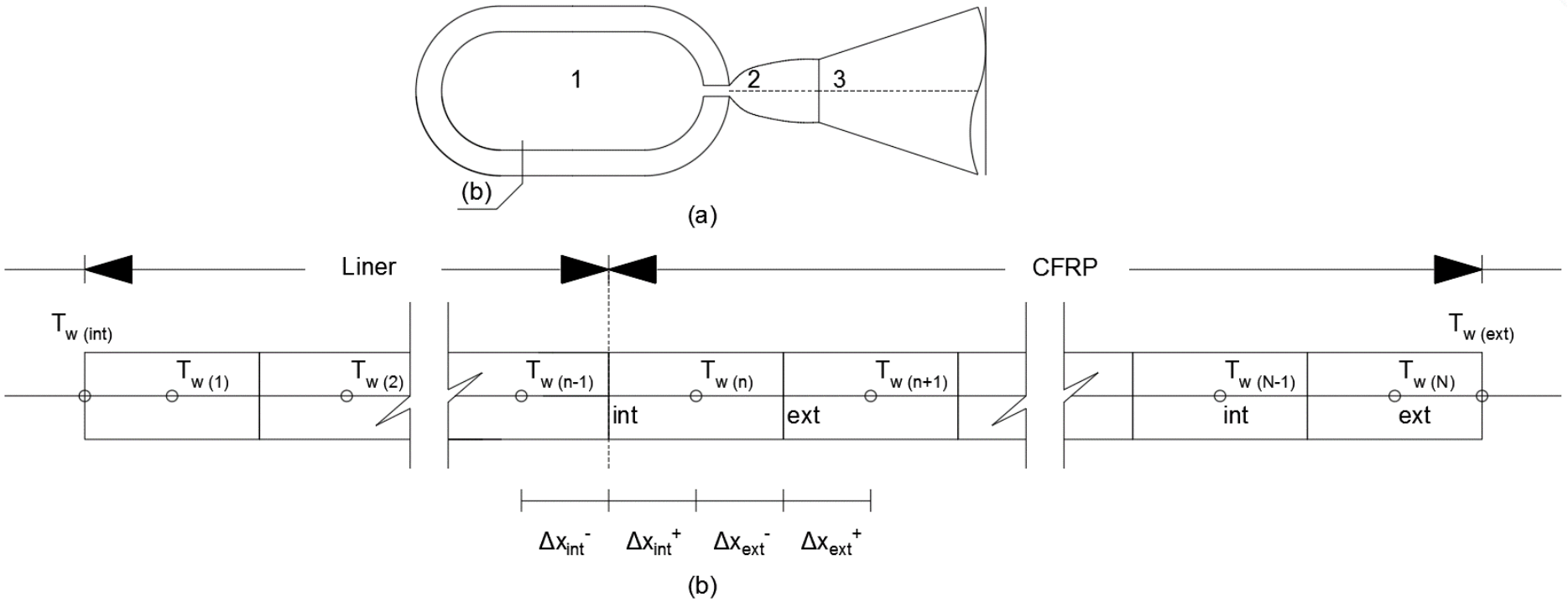

Figure 1. Schematic diagram of the pressurised tank: (a) 1. inside the tank 2. at the orifice exit 3. at the notional nozzle, (b) tank wall.

2.1 Inside the Tank

The first equation in the model is the first law of thermodynamic as Eq. 1 where energy variation inside the tank is due to the heat transfer to the system from the surroundings and the outgoing enthalpy.

$$\frac{\Delta U}{\Delta t} = \frac{\Delta Q}{\Delta t} - h_{out}\dot{m}, \tag{1}$$

where U (J) is the total internal energy in the tank, Q (J) is the heat into the system due to the surrounding, h_{out} (J/kg) is the enthalpy going out from the system ($h_{out} = c_{p,g}T_1$) and $\dot{m}$ (kg/s) is the mass flow rate. The value of $\frac{\Delta Q}{\Delta t}$ in Eq. 1 is given as [8]

$$\frac{\Delta \mathrm{Q}}{\Delta \mathrm{t}} = k_{int}A_{int}(T_{w(int)} - T_1), \tag{2}$$

where T_1 (K) is the gas temperature inside the tank (assumed to be homogenous), $T_{w(int)}$ (K) is the temperature of the inside surface of the tank wall, k_{int} (W/m^2/K) is the heat transfer coefficient between the inside gas and the internal surface of the tank wall and A_{int} (m^2) is the internal area of the tank. The value of U in Eq. 1 is given as [9]

$$U = \frac{P_1(V - m_1 b)}{\gamma - 1}, \tag{3}$$

where P_1 (Pa) is the pressure of the gas inside the tank, m_1 (kg) is the mass of the gas inside the tank, V_1 (m^3) is the volume of the tank, b (m^3/kg) is the co-volume constant of the gas [10] and γ (-) is the specific heat ratio of the gas. Finally, the gas temperature inside the tank is calculated with the Abel-Noble equation of state [11, 2]

$$T_1 = \frac{P_1(1 - b\rho_1)}{\rho_1 R_g}, \tag{4}$$

where ρ_1 (kg/m^3) is the density of the gas inside the tank and Rg (m^2.s^2/K) is the gas constant.

2.2 Orifice and Notional Nozzle

Under expanded jet theory of [1, 2] is used for the calculation of parameters at the orifice and notional nozzle. To find the density at the orifice, transcendental equation of isentropic expansion [2] is solved as

$$\left[\frac{\rho_1}{1 - b\rho_1}\right]^{\gamma} = \left[\frac{\rho_2}{1 - b\rho_2}\right]^{\gamma} \cdot \left[1 + \left(\frac{\gamma - 1}{2(1 - b\rho_2)^2}\right)\right]^{\gamma/\gamma - 1}, \tag{5}$$

where ρ_2 (kg/m^3) is the density of the gas at the orifice. Then, energy conservation equation between inside the tank and the orifice is used to calculate the temperature of the gas at the orifice [2]

$$\frac{T_1}{T_2} = 1 + \frac{\gamma - 1}{2(1 - b\rho_2)^2}, \tag{6}$$

where T_2 (K) is the temperature of the gas at the orifice. Abel-Noble equation of state [11] is used for the calculation of pressure at the orifice (P_2) as

$$P_2 = \frac{\rho_2 R_g T_2}{1 - b\rho_2}. \tag{7}$$

Considering the chocked flow at the orifice, the gas velocity is assumed to be equal to the local sound velocity, hence the velocity (u_2) is calculated by using the equation for the sound velocity [11, 2] as

$$u_2 = \frac{\left(\gamma R_g T_2\right)^{0.5}}{1 - b\rho_2}. \tag{8}$$

Energy conservation equation between the orifice and the notional nozzle is used for the calculation of the temperature at the notional nozzle (T_3) as Eq. 9. It must be mentioned that the velocity of the gas at the notional nozzle is assumed to be equal to the local sound velocity [1, 2].

$$T_3 = \frac{2T_2}{\gamma + 1} + \frac{(\gamma - 1)}{(\gamma + 1)} \cdot \frac{P_2}{\rho_2(1 - b\rho_2)R_g}. \tag{9}$$

Considering the gas pressure at the notional nozzle equal to the ambient pressure (P_{amb}), Abel-Noble equation of state [11] is used to calculate the density at the notional nozzle (ρ_3) as

$$\rho_3 = \frac{P_{amb}}{P_{amb}b + R_g T_3}. \tag{10}$$

The same as the gas velocity calculation for the orifice (Eq. 8), it is assumed that the gas velocity at the notional nozzle is equal to the local sound velocity and it is calculated as

$$u_3 = \frac{\left(\gamma R_g T_3\right)^{0.5}}{1 - b\rho_3}. \tag{11}$$

Finally, the continuity equation between the orifice and the notional nozzle is used to calculate the diameter of the notional nozzle (Eq. 12) followed by the mass flow rate calculation (Eq. 13) as

$$D_3 = D_2 \sqrt{C_D \frac{\rho_2 u_2}{\rho_3 u_3}}, \tag{12}$$

$$\dot{m} = \frac{\rho_3 u_3 \pi (D_3)^2}{4}, \tag{13}$$

where D_2 (m) is the orifice diameter, D_3 (m) is the notional nozzle diameter and C_D is the discharge coefficient. At each time step, $\dot{m}$ is updated and is used as an input for Eq. 1.

2.3 Tank Wall (Fig. 1b)

Assuming the wall to behave as a one-dimensional solid, the conservation of energy within the wall can be determined by unsteady heat conduction equation (Eq. 14) [6].

$$\rho_w c_{pw} \frac{dT_w}{dt} = \frac{d}{dx}\left(\lambda_w \frac{dT_w}{dx}\right) + S, \tag{14}$$

where ρ_w (kg/m^3) is the density of the wall, c_{pw} (J/kg/K) is the specific heat capacity of the wall, T_w (K) is the temperature of wall, λ_w (W/m/K) is the thermal conductivity of the wall, x (m) is the wall thickness, and S is the heat source term within the wall. Considering the grid-point cluster in Fig. 1b, Eq. 14 is integrated in the form of

$$\rho_{w(n)} c_{w(n)} \frac{dT_{w\,(n)}}{dt} \Delta x = \left(\lambda_w \frac{dT_{w\,(n)}}{dx}\right)_{ext} - \left(\lambda_w \frac{dT_{w\,(n)}}{dx}\right)_{int} + \int_{int}^{ext} S dx, \tag{15}$$

where subscript *n* for each parameter is the grid-point number and subscripts *int* and *ext* are representatives for internal surface and external surface of the wall, respectively (Fig. 1b). $\int_{int}^{ext} S \times dx$ is the heat source term and it is assumed to be zero at this stage of the current study. A piecewise-linear profile is employed to obtain the derivatives $dT_{w(n)}/dx$ [6] and finite difference solution method is used to solve the right-hand side of Eq. 15 as

$$\rho_{w(n)} c_{w(n)} \Delta x \frac{T_{w(n)}^{i} - T_{w(n)}^{i-1}}{\Delta t} = \frac{T_{w(n+1)}^{i-1} - T_{w(n)}^{i-1}}{\frac{\Delta x_{ext}^{-}}{\lambda_{ext}^{-}} + \frac{\Delta x_{ext}^{+}}{\lambda_{ext}^{+}}} - \frac{T_{w(n)}^{i-1} - T_{w(n-1)}^{i-1}}{\frac{\Delta x_{int}^{-}}{\lambda_{int}^{-}} + \frac{\Delta x_{int}^{+}}{\lambda_{int}^{+}}}, \tag{16}$$

where superscript i is the iteration number at each time step, Δx_{ext}^{-} (m) is the distance from grid point n to the external surface of the control volume, Δx_{ext}^{+} (m) is the distance from the external surface of the control volume to the grid point n+1, Δx_{int}^{-} (m) is the distance from the internal surface of the control volume to the grid point n-1, Δx_{int}^{+} (m) is the distance from grid point n to the internal surface of the control volume, λ_{ext}^{-} (W/m/K) is the thermal conductivity of the wall between grid point n and the external surface of the control volume, λ_{ext}^{+} (W/m/K) is thermal conductivity of the wall between the external surface of the control volume and grid point n+1, λ_{int}^{-} (W/m/K) is the thermal conductivity of the wall between the internal surface of the control volume and grid point n-1 and λ_{int}^{+} (W/m/K) is the thermal conductivity of the wall between grid point n and the internal surface of the control volume.

Considering the balance of convection and conduction on the surfaces, the temperatures of the surfaces of the wall are calculated as

$$q_{convection}^{"} = q_{conduction}^{"} \quad (internal) \quad \Rightarrow \quad -\lambda_w \frac{dT_{w\,(n)}}{dx}\bigg|_{n=int} = k_{int}\left(T_1 - T_{w\,(n)|n=int}\right), \tag{17}$$

$$q_{convection}^{"} = q_{conduction}^{"} \quad (external) \Rightarrow \quad -\lambda_w \frac{dT_{w\,(n)}}{dx}\bigg|_{n=ext} = k_{ext}\left(T_{w\,(n)|n=ext} - T_{amb}\right), \tag{18}$$

where k_{int} (W/m^2/K) and k_{ext} (W/m^2/K) are heat transfer coefficients of the internal and external surface of the wall, respectively. Equations 17 and 18 are solved in the form of

$$-\frac{1}{\frac{\Delta x_{int}^{+}}{\lambda_{int}^{+}}}\left(T_{w(1)} - T_{w(int)}\right) = k_{int}\left(T_1 - T_{w(int)}\right), \tag{19}$$

$$-\frac{1}{\frac{\Delta x_{ext}^{-}}{\lambda_{ext}^{-}}}\left(T_{w(N)} - T_{w(ext)}\right) = k_{ext}\left(T_{amb} - T_{w(ext)}\right), \tag{20}$$

where $T_{w(1)}$ (K) is the temperature of the first grid point after the wall internal surface, $T_{w(N)}$ (K) is the temperature of the last grid point before the wall external surface, $T_{w(int)}$ (K) is the temperature of the internal surface of the wall, $T_{w(ext)}$ (K) is the temperature of the external surface of the wall and T_{amb} (K) is the ambient temperature.

Heat transfer coefficients k_{int} and k_{ext} are important parameters during the convective heat transfer from the inside gas to the internal surface of the wall and from the ambience to the external surface of the wall. In our study, Nusselt number correlations for forced and natural convection, suggested by [7], were employed to estimate the heat transfer coefficients in each time step. For the internal surface of the tank wall, k_{int} is estimated as

$$Nu_{Din} = \frac{D_{int} \times k_{int}}{\lambda_g} = 0.104 (Ra_{int})^{0.352}, \tag{21}$$

where Nu_{Din} (-) is the Nusselt number of the inside gas, D_{int} (m) is the internal diameter of the tank, λ_g (W/m/K) is the thermal conductivity of the inside gas and Ra_{int} (-) is the Rayleigh number of the inside gas which is calculated as

$$Ra_{Din} = \frac{g\beta\left|T_1 - T_{w(int)}\right|c_{p,g}(\rho_1)^2 D_{int}^3}{\mu_g \lambda_g}, \tag{22}$$

where g (m/s^2) is the acceleration due to gravity, β (1/K) is the thermal expansion coefficient of the gas, $c_{p,g}$ (J/kg/K) is the specific heat capacity of the gas and μ_g (Pa.s) is the dynamic viscosity of the gas. For the external surface of the tank wall, k_{ext} is estimated as

$$Nu_{Dext} = \frac{k_{ext} D_{ext}}{\lambda_{air}} = \left(0.4 Re_{Dext}^{0.5} + 0.06 Re_{Dext}^{\frac{2}{3}}\right) Pr_{air}^{0.4}, \tag{23}$$

where Re_{Dext} (-) is the Reynolds number of the air and Pr_{air} (-) is the Prandtl number of the air which are calculated as

$$Re_{Dext} = \frac{\rho_{air} V_{air} D_{ext}}{\mu_{air}}, \tag{24}$$

$$Pr_{air} = \frac{\mu_{air} c_{p,air}}{\lambda_{air}}, \tag{25}$$

where ρ_{air} (kg/m^3) is the density of the air, D_{ext} (m) is the external diameter of the tank, μ_{air} (Pa.s) is the dynamic viscosity of the air, $c_{p,air}$ (J/kg/K) is the specific heat capacity of the air and λ_{air} (W/m/K) is the air conductivity. The experiment of validation for the current study was performed in HYKA-HyJet research facility at Karlsruhe Institute of Technology (KIT) in an enclosed environment with no air velocity. The external wall of the tank is exposed to the constant ambient temperature. According to [7] and [12], in such condition, the effect of the external heat transfer coefficient on inside gas temperature is negligible if not zero. Thus, in the current study, the value of the air velocity (V_{air}) was assumed to be 8 m/s as [5].

2.4 Input Parameters and Initial Conditions

Input and output parameters of the model are presented in Table 1. Initial density in the tank is calculated by employing Abel-Noble equation of state as [2, 11]

$$\rho_1^0 = \frac{P_1^0}{P_1^0 \cdot b + R_g \cdot T_1^0}, \tag{26}$$

and the initial mass in the tank is obtained as

$$m_1^0 = V \cdot \rho_1^0. \tag{27}$$

Table 1. Inputs and outputs of the blowdown model.

Input parameters	
Tank	V, D_{int}, D_{ext}, D_2, A_{int}, λ_{CFRP}, λ_{Liner}, ρ_{CFRP}, ρ_{Liner}, $c_{p,CFRP}$, $c_{p,Liner}$
Inside gas	$c_{p,g}$, $c_{v,g}$, λ_g, β, R_g, γ, b, M_g, μ_g
Air	μ_{air}, $c_{p,air}$, λ_{air}, ρ_{air}, V_{air}

Initial conditions	$P_{amb},\ T_{amb},\ P_1^0,\ T_1^0,\ T_{w(1)}^0\ to\ T_{w(N)}^0,\ T_{w(int)}^0,\ T_{w(ext)}^0$
Output parameters	
Inside the tank	$m_1^i, \rho_1^i, P_1^i, T_1^i$
Orifice exit	$\rho_2^i, T_2^i, P_2^i, u_2^i$
Notional nozzle	$T_3^i, \rho_3^i, u_3^i, D_3^i, \dot{m}^i$
Tank wall	$k_{int}^i, k_{ext}^i, T_{w(n)}^i, T_{w(int)}^i, T_{w(ext)}^i$

ρ_2^0, T_2^0, P_2^0 and u_2^0 are obtained by employing Eq. (5)-Eq. (8), respectively. T_3^0, ρ_3^0, u_3^0, D_3^0 and $\dot{m}^0$ are calculated through Eq. (9)-Eq. (13) and k_{int}^0 and k_{ext}^0 are computed by using Eq. (21) and Eq. (23). During the simulation, at each time step, mass (m_1^i) and density (ρ_1^i) inside the tank are updated as

$$m_1^i = m_1^{i-1} - \dot{m}^{i-1} \cdot \Delta t, \tag{28}$$

$$\rho_1^i = \frac{m_1^i}{V}, \tag{29}$$

and the output parameters are obtained by employing Eq. (1)-Eq. (25).

3.0 EXPERIMENT OF VALIDATION

3.1 KIT Experiment

Experiment of validation took place in HYKA-HyJet research facility at Karlsruhe Institute of Technology (KIT). An impinging jet test platform was made, which included a high-pressure storage tank type IV (19 litre) connected to a release nozzle with 1 mm diameter. The storage vessel was firstly charged to 700 bar by helium gas and then cooled down to a normal room temperature (293 K) before start of the blowdown. Tank characteristics were not available and for this study the required parameters were extracted from a similar tank [13] as explained in Table 2. Inside temperature was measured by a thermocouple installed in the middle of the high pressure tank. Pressure change inside the tank was also measured during the blowdown.

Table 2. Dimensions and properties of tank.

Type IV tank [13]	
Internal volume (L)	19
Internal diameter (mm)	180
External diameter (mm)	228
External length	904
HDPE liner [14, 13]	
Thickness (mm)	7
Thermal conductivity (W/m/K)	0.385
Specific heat capacity (J/kg/K)	1584
Density (kg/m^3)	945
CFRP [15, 16]	
Thickness (mm)	17
Thermal conductivity (mm)	0.5
Specific heat capacity (J/kg/K)	1020
Density (kg/m^3)	1360

3.2 Input Parameters

Helium was stored at the pressure of 70 (MPa) in a 19 litre type IV tank. The input parameters to be used for the calculation in each time step are presented in Table 3.

Table 3. Input parameters for blowdown of helium (70 MPa, 19 Litre tank type IV).

Parameter	Unit	Value	Reference
$c_{p,g}$	J kg^{-1} K^{-1}	5.22·10^{3}	[17]
$c_{v,g}$	J kg^{-1} K^{-1}	3.15·10^{3}	[17]
γ	-	1.66	[17]
P_1^0	Pa	7.00·10^{7}	
T_1^0	K	293	
R_{He}	m^2 s^2 K^{-1}	2.08·10^{3}	[17]
b	m^3 kg^{-1}	2.67·10^{-3}	[10]
g	m s^{-2}	9.81	
μ_{air}	Pa s	1.98·10^{-5}	[18]
$c_{p,air}$	J kg^{-1} K^{-1}	1.01·10^{3}	[18]
λ_{air}	W m^{-1} K^{-1}	2.57·10^{-2}	[18]
ρ_{air}	kg m^{-3}	1.21	[18]
T_{amb}	K	293	
P_{amb}	Pa	1.01·10^{5}	

For different pressure and temperature at each time step, the values of helium conductivity (λ_g), dynamic viscosity (μ_g), and thermal expansion (β) coefficient were interpolated based on National Institute of Standards (NIST) database. Abel-Noble equation of state was employed for the calculation of initial density of the gas in the vessel as 8.80·10^{1} (kg/m^3) and the initial mass as 1.67 (kg). Equations 1 to 25 were then used in a timely basis to calculate the required parameters.

4.0 RESULTS AND DISCUSSION

Figure 2 demonstrates the comparison between the corresponding results for the measured gas pressure with those simulated by both adiabatic blowdown model [1] and non-adiabatic blowdown model (new model). It must be mentioned that for the simulation for either adiabatic blowdown model and non-adiabatic blowdown model (new model) the discharge coefficient (C_D) of 0.9 was used as in [19] which showed the best fit of the results. At the beginning of the blowdown, when there is not much heat transfer through the wall, both models are in a good agreement with the experimental values. By continuing the venting, the adiabatic blowdown model predicts a faster decrease of pressure than those measured by the experiment. Rapid pressure drop due to the simulation by the adiabatic model was also reported by [3, 1]. As demonstrated in Fig. 2, one can observe that the simulated gas pressure with non-adiabatic model (new model) is in an excellent agreement with the experiment.

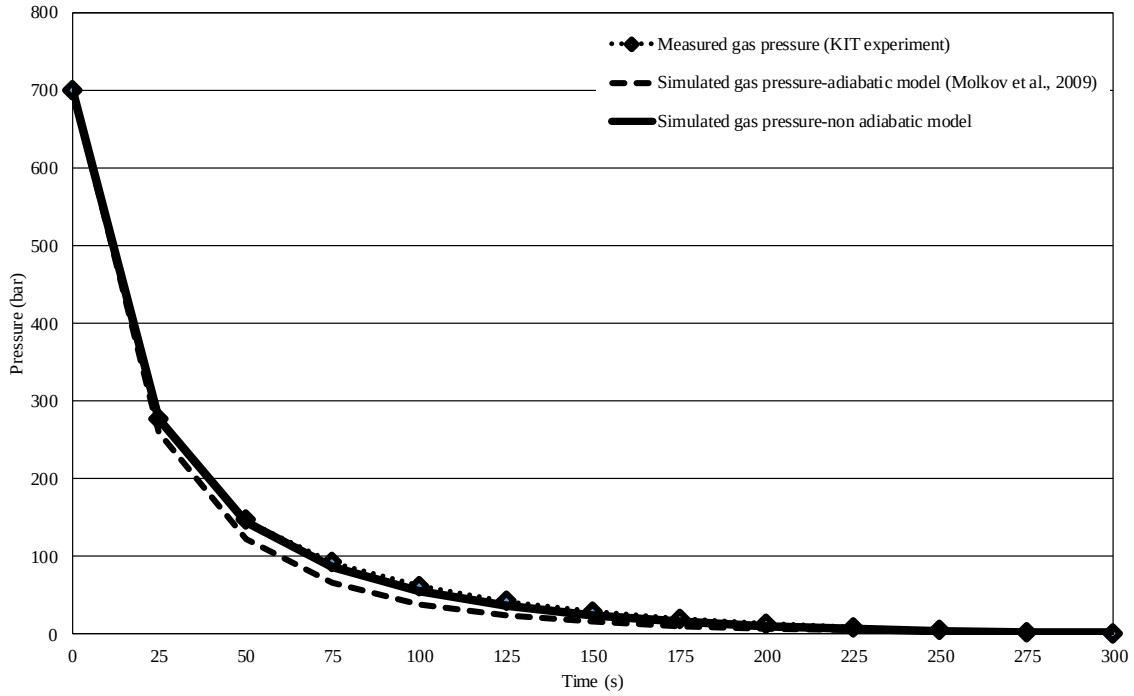

Figure 2. Measured pressure in helium gas discharge in comparison to simulated pressure with both adiabatic (Molkov et al., 2009) and non-adiabatic blowdown model.

For the temperature prediction, the effects of heat transfer through the wall is significant (Fig. 3). When the gas starts to vent, the temperature predicted by the adiabatic blowdown model [1] is in an agreement with the experiment. However, after few seconds, in adiabatic condition the gas inside the tank continues to cool down fast while the rate of the temperature drop is slower as per experimental results.

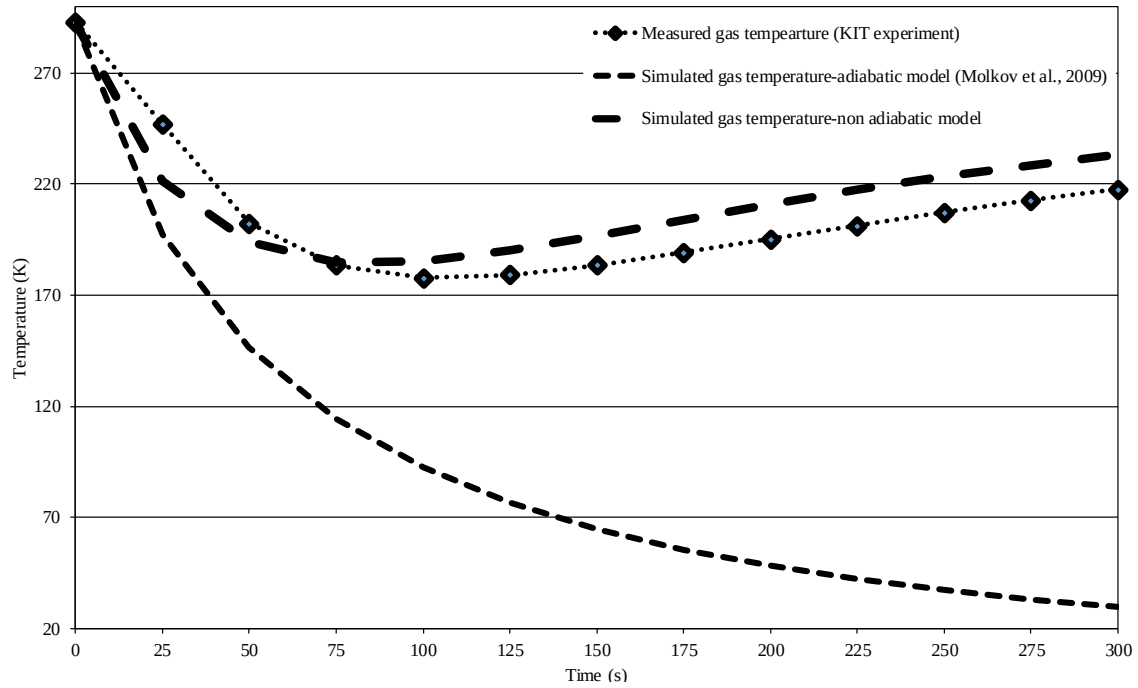

Figure 3. Measured temperature of helium gas discharge in comparison to simulated temperature with both adiabatic (Molkov et al., 2009) and non-adiabatic blowdown model.

In fact, the heat transfer through the wall prevents the quick decrease of the gas temperature and even warms up the inside gas after around 100 seconds of gas discharge from the vessel. It is demonstrated in Fig. 3 that simulated temperature by the adiabatic model continues to decrease until the end of the discharge and it is not in any agreement with the measured values. In this case, the non-adiabatic blowdown model is in better agreement with experiment. As Fig. 3, at the beginning of the blowdown, the rate of temperature drop calculated by non-adiabatic model is slower than assuming the adiabatic condition. As explained in section 1, the heat transfer through the wall during the blowdown is due to two competing waves of temperature. When the venting starts, the decompression of the inside gas causes the slow temperature drop and the heat transfer from the ambience is not in effect yet. However, after a certain time, the inside temperature of the tank starts to rise due to dominant heat transfer from the ambience. This trend is in an agreement with the measured values by the experiment.

As demonstrated in Fig. 3, during the first 75 (s) of the blowdown, the non-adiabatic model predicts a faster temperature drop than the experiment. To evaluate the later underprediction, one must understand the thermocouple performance. According to KIT experimental facility, the thermocouple which is used in the experiment needs sometimes to react. Its sensitive tip consists of two wires that are from different materials and are welded together. The tip is shielded against the environmental effects by a thin layer of magnesium oxide and the whole thing is covered by a thin steel shell. This brings some delay in thermocouple response which is difficult to determine. The whole thing is again located in a metal fitting and it prevents the direct contact of thermocouple with the gas, hence there is an extra barrier with consequent additional delay. This delay is the main reason for the slower temperature drop which is monitored in the measured temperature (Fig. 3).

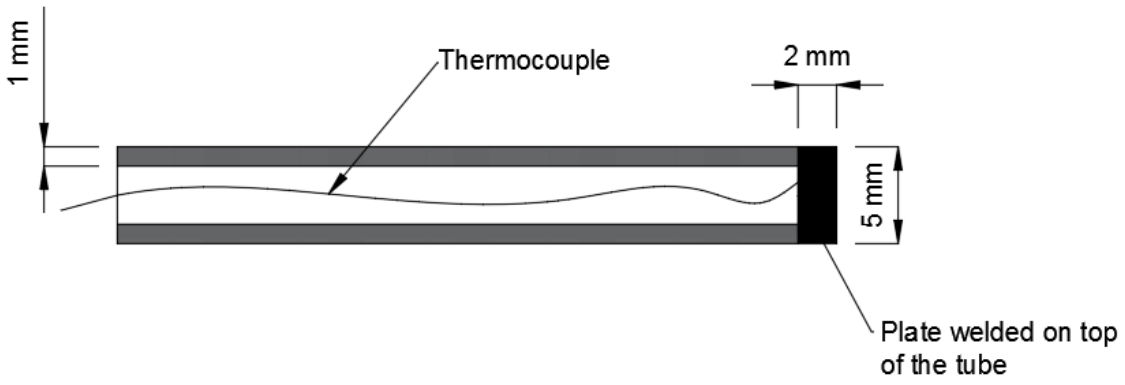

Figure 4. Schematic diagram of the thermocouple and the corresponding metal tube.

The schematic diagram of the thermocouple and the metal fitting around is demonstrated in Fig. 4 which was provided by private communication with the KIT experimental facility. The metal fitting material is steel 1.4571. To consider the delay due to the metal tube around the thermocouple, the lumped heat transfer model (Eq. 26) was employed. The delay was considered to be due to the heat transfer through the metal plate (2 mm thickness; 5 mm diameter) welded on top of the tube, thus at each time step, the corresponding temperature was considered to be the same as that of metal plate.

$$\frac{T_1^i - T_{plate}^i}{T_1^i - T_{plate}^{i-1}} = exp\left(-\frac{k_{plate}^{i-1} A}{\rho_{plate} c_{p,plate} V_{plate}} \cdot \Delta t\right), \tag{30}$$

where T_1 (K) is the inside gas temperature at each time step, T_{plate} (K) is the metal plate temperature at each time step, k_{plate} (W/m^2/K) is the heat transfer coefficient of the external surface of the plate, A (m^2) is the area of the metal plate which is in contact with the inside gas, ρ_{plate} (kg/m^3) is the density of the metal plate, $c_{p,palte}$ (J/kg/K), V_{plate} (m^3) is the volume of the plate and Δt (s) is the duration of each time step. To consider the lumped heat transfer model (Eq. 30), one must make sure that the solid is thermally thin: a sloid is thermally thin when the relation ($Biot\ number = k_{plate} \times L/\lambda_{plate} \leq 0.1$)

is met. λ_{plate} (W/m/K) is the conductivity of the metal plate and L (m) is its thickness. Heat transfer coefficient (k_{plate}) at each time step is calculated based on the Nusselt number correlation of [20] as

$$Nu_{plate} = \frac{D_{plate} k_{plate}}{\lambda_g} = 0.54\left(Ra_{plate}\right)^{0.25}, \tag{31}$$

$$Ra_{plate} = \frac{g\beta\left|T_1 - T_{plate}\right| c_{p,g} (\rho_1)^2 D_{plate}^3}{\mu_g \lambda_g}, \tag{32}$$

where D_{plate} (m) is the diameter of the metal plate (5 mm). The properties of the metal plate (steel 1.4571) was considered as ρ_{metal}= 7.90·10^3 (kg/m^3), $c_{p,metal}$= 480 (J/kg/K) and λ_{metal}= 16 (W/m/K) [18]. It must be mentioned that the use of Eq. 31 is advised for the laminar convection when the Ra number (Eq. 32) is less than 10^7 [20]. The values of Biot number and Rayleigh number (Ra_{plate}) in each time step is calculated and demonstrated in Fig. 5.

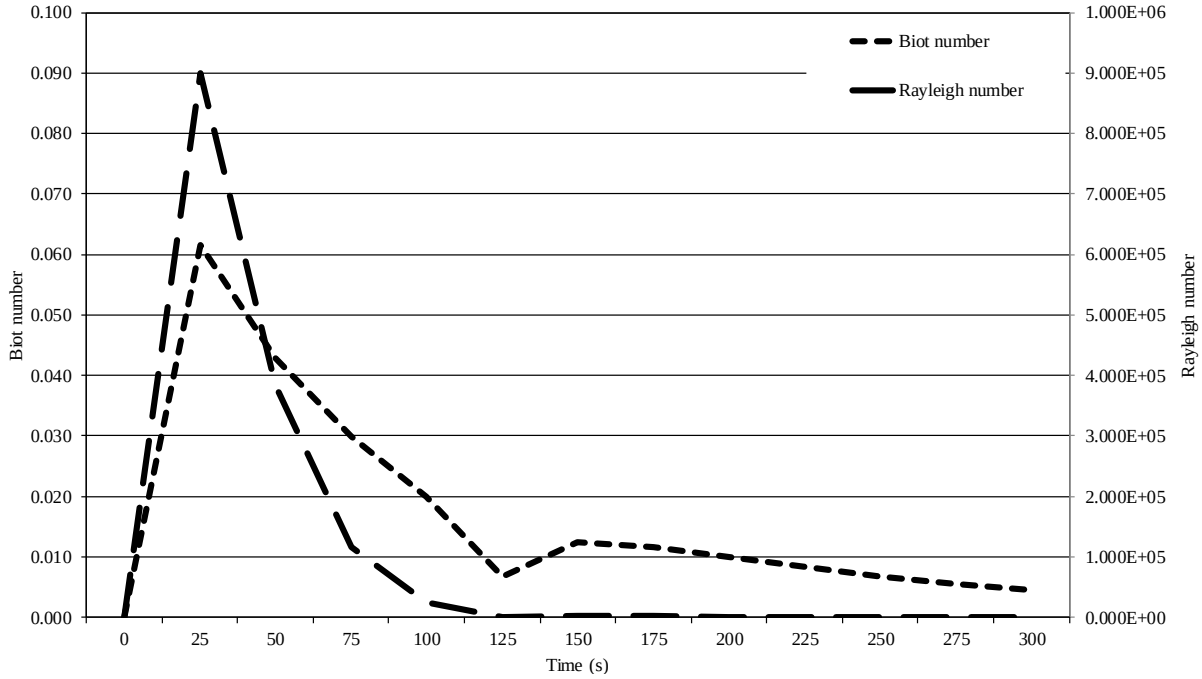

Figure 5. Biot number (Bi) and Rayleigh number (Ra) of the welded metal plate on top of the thermocouple tube during the discharge duration.

One can observe that the Biot number during the entire discharge time is less than 0.1, hence the metal plate can be considered as thermally thin and the condition for considering the lumped heat transfer model (Eq. 26) is met. The values of Rayleigh number are also in an acceptable range (< 10^7) to use the Nusselt number correlation as Eq. 27.

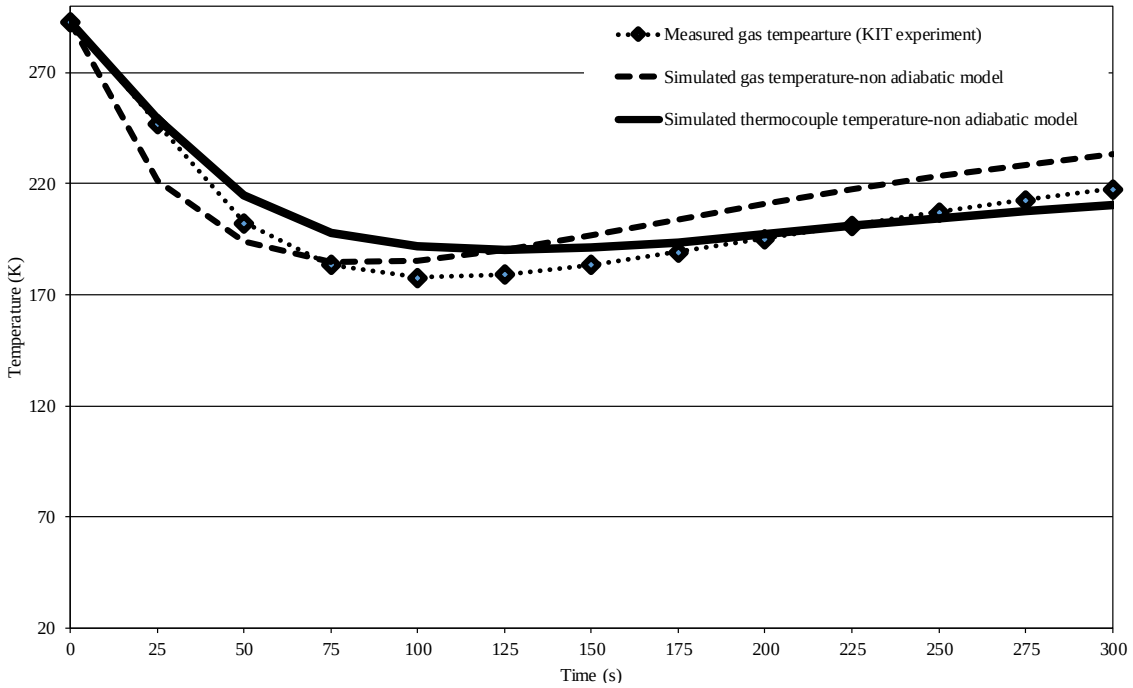

Figure 6. Measured temperature in helium gas discharge in comparison to simulated temperature with non-adiabatic blowdown model, considering the thermocouple delay.

In each time step, Eq. 30-Eq. 32 were employed to calculate the temperature of the thermocouple due to delayed response (Fig. 6). It is observed that the temperature drops with a lower rate in thermocouple and it is in better agreement with the experiments (around 7% error).

The developed novel blowdown model predicts the dynamic pressure and temperature of the gas during the blowdown. Doing so makes the model able to be used for the optimizing the TPRD design parameters, i.e. time to activation and the optimum diameter of the orifice. Fast simulation time and its flexibility to be performed on non-high performance computers makes the model to be implemented as a complimentary tool for the inherent safer design of tank-TPRD systems. In combination with CFD modeling, the model can also be a reliable pre-processor and the predicted values may be used as input parameters for the simulation which makes the CFD computation time efficient. The model however is still under development and there are still various tasks to be considered. It must be mentioned that the thermal properties of the storage vessel wall are important and they were not available from the experimental facility and these values were extracted from other studies. The heat transfer coefficients for both tank wall and the metal plated welded to the thermocouple are also very important parameters which was calculated based on Nusselt correlation suggested by similar studies. However, to evaluate the accurate thermodynamic behavior of the inside gas and the tank structure, more comprehensive experimental results are required. Detailed information with regards to the tank dimensions and wall thickness, the physical and thermal properties of CFRP and liner used in the tank and their thickness are required. The temperature change on the surface of the tank and within the wall, during the discharge, is also of interest as it can be used to estimate the heat transfer coefficients.

5.0 CONCLUSION

A novel engineering tool was developed which is capable of predicting the thermodynamic behavior of extremely high pressurized gas storage tanks during the blowdown. Energy conservation of equation and Abel-Noble equation of state were employed to predict the dynamic pressure and temperature inside the tank. The underexpanded jet theory was used to evaluate the pressurized gas behavior after venting of the tank. To consider the heat transfer through the tank wall, one dimensional unsteady heat transfer equation was introduced and formulated to take into account the thermal properties of a composite tank

wall. The finite difference method was employed to solve the system of equations. At each time step, Nusselt number correlations for forced and natural convection were employed to compute the heat transfer coefficients for the external and internal surfaces of the tank wall. The model was validated against the KIT experiment (helium blowdown; 70 MPa; 19 liter tank type IV): the dynamic pressure and temperature simulated by the model were in an excellent agreement with the experiment (around 7% error). Avoiding the expensive/risky experiments and long CFD simulation time makes the model cost effective and time efficient. The model will be used as a complimentary tool for design of inherently safer tank-TPRD system. It must be mentioned that a more detailed evaluation of convective heat transfer through different parts of the tank structure and during the fire is still required and is under investigation.

ACKNOWLEDGEMENTS

The authors are grateful to Engineering and Physical Sciences Research Council (EPSRC) for funding through SUPERGEN H2FC Hub (EP/J016454/1 and EP/P024807/1) and SUPERGEN Challenge "Integrated safety strategies for onboard hydrogen storage" (EP/K021109/1) projects. This study has received funding from the Fuel Cell and Hydrogen 2 Joint Undertaking under grant agreement No.736648 (NET-Tools project). This Joint Undertaking received support from the European Union's Horizon 2020 research and innovation programme and Hydrogen Europe and N. ERGHY. Authors thankfully acknowledge Dr. Andreas Friedrich from HYKA-HyJet research facility at KIT (Germany) for his valuable consulting support.

REFERENCES

1. V. Molkov, D. Makarov and M. Bragin, "Physics and modelling of under-expanded jets and hydrogen dispersion in atmosphere," *Physics of Extreme State of Matter*, pp. 143-145, 2009.

2. V. Molkov, Fundamentals of hydrogen safety engineering, bookboon.com, 2012.

3. R. W. Schefer, W. G. Houf, T. C. Williams, B. Bourne and J. Colton, "Characterization of high-pressure, underexpanded hydrogen-jet flames," *International Journal of Hydrogen Energy*, vol. 32, no. 12, pp. 2081-2093, 2007.

4. S. Brennan and V. Molkov, "Safety assessment of unignited hydrogen discharge from onboard storage in garages with low levels of natural ventilation," *International Journal of Hydrogen Energy*, vol. 38, no. 19, p. 8159–8166, 2013.

5. T. Bourgeoise, F. Ammouri, M. Weber and C. Knapik, "Evaluating the temperature inside a tank during a filling with highly-pressurized gas," *International Journal of Hydrogen Energy*, vol. 40, no. 35, pp. 11748-11755, 2015.

6. S. Patankar, Numerical heat transfer and fluid flow (Series in computational methods in mechanics and thermal sciences), New York: McGRAW-HILL BOOK COMPANY, 1980.

7. P. Woodfield, M. Monde and T. Takano, "Heat tranfer charateristics for practical hydrogen vessels being filled at high pressure," *Journal of Thermal Science and Technology*, vol. 3, no. 2, pp. 241-253, 2008.

8. M. Monde, P. Woodfield, T. Takano and M. Kosaka, "Estimation of temperature change in practical hydrogen pressure tanks being filled at high pressures of 35 MPa and 70 MPa," *International Journal of Hydrogen Energy*, vol. 37, no. 7, pp. 5723-5734, 2012.

9. V. Molkov and S. Kashkarov, “Blast wave from a high-pressure gas tank rupture in a fire: Stand-alone and under-vehicle hydrogen tanks,” *International Journal of Hydrogen Energy*, vol. 40, no. 36, p. 12581–12603, 2015.

10. D. Chenoweth, “Gas-transfer analysis. Section H-Real gas results via the van der Waals equation of state and viral-expansion extensions of its limiting Abel-Noble form,” Sandia National Laboratories, Livermore, CA, 1983.

11. I. Johnson, “The Noble-Abel equation of state: thermodynamic derivations for ballistics modelling.,” Weapons Systems Division, Defence Science and Technology Organisation. DSTO-TN-0670, 2005.

12. M. Heitsch, D. Baraldi and P. Moretto, “Numerical investigations on the fast filling of hydrogen tanks,” *International Journal of Hydrogen Energy*, vol. 36, pp. 2606-2612, 2011.

13. B. Acosta, P. Moretto, N. de Miguel, R. Ortiz, F. Harskamp and C. Bonato, “JRC reference data from experiments of on-board hydrogen tanks fast filling,” *International Journal of Hydrogen Energy*, vol. 39, no. 35, pp. 20531-20537, 2014.

14. M. Monde and M. Kosaka, “Understanding of thermal characteristics of fueling hydrogen high pressure tanks and governing parameters,” *SAE International Journal of Alternative Powertrains*, vol. 2, no. 1, pp. 61-67, 2013.

15. J. Hidalgo, P. Pironi, R. Hadden and S. Welsh, “Effect of thickness on the ignition behaviour of carbon fibre composite materials used in high pressure vessels,” in *Proceedings of the Eight International Seminar on Fire and Explosion Hazards (ISFEH8)*, Hefei, China, 2016.

16. S. Welsh, R. Hadden, J. Hidalgo and P. Pironi, *Thermal properties and thermal modelling of composite materials exposed to fires*, 2017.

17. NIST, “Isothermal properties for helium,” 2016. [Online]. Available: http://webbook.nist.gov/cgi/fluid.cgi?T=293&PLow=0&PHigh=70&PInc=&Applet=on&Digits=5&ID=C7440597&Action=Load&Type=IsoTherm&TUnit=K&PUnit=MPa&DUnit=mol%2Fl&HUnit=kJ%2Fmol&WUnit=m%2Fs&VisUnit=uPa*s&STUnit=N%2Fm&RefState=DEF. [Accessed 2017].

18. The Engineering ToolBox, “Resources, tools and basic information for engineering and design of technical applications,” 2017. [Online]. Available: http://www.engineeringtoolbox.com/index.html. [Accessed 2017].

19. M. Kuznetsov, S. Pariest, A. Friedrich, G. Stern and J. Travis, “Experimental investigation of non-ideality and non-adiabatic effects under high pressure releases,” *International Journal of Hydrogen Energy*, pp. 16398-16407, 2015.

20. F. Incropera and D. De Witt, Fundamentals of heat and mass transfers, 2nd ed., New York: John Wiley and Sons Inc, 1985.

21. W. S. Winters, “TOPAZ—a computer code for modeling heat transfer and fluid flow in arbitrary networks of pipes, flow branches, and vessels. SAND83-8253,” Sandia National Laboratories, Livermore, CA, 1984.